

# Experimental study of a radial mode thermoacoustic prime mover

Jay A. Lightfoot

*Dynetics, Inc., 1000 Explorer Boulevard, Huntsville, Alabama 35759*

W. Patrick Arnott

*Atmospheric Science Center, Desert Research Institute, P.O. Box 60220, Reno, Nevada 89506*

Henry E. Bass and Richard Raspet

*National Center for Physical Acoustics and Department of Physics and Astronomy,*

*University of Mississippi, University, Mississippi 38677*

(Received 10 June 1998; revised 10 December 1998; accepted 11 December 1998)

The purpose of this research is to branch out from thermoacoustics in the plane wave geometry to study radial wave thermoacoustic engines. The radial wave prime mover is described. Experimental results for the temperature difference at which oscillations begin are compared with theoretical predictions. Predictive models often assume a uniform pore size and temperature continuity between the stack and heat exchangers; however, stacks of nonuniform pore size and temperature discontinuities between the stack and heat exchangers are common imperfections in experimental devices. The radial engine results are explained using a theoretical model which takes into account these prevalent construction flaws. Theory and experiment are shown to be in agreement after the complications are included. Spectral measurements show that an additional feature of the radial geometry is the anharmonicity of the resonant modes which significantly reduces nonlinear harmonic generation. © 1999 Acoustical Society of America. [S0001-4966(99)05603-9]

PACS numbers: 43.35.Ud, 43.20.Bi [ANN]

## INTRODUCTION

The primary goal of this paper is to examine an experimental radial wave thermoacoustic engine, taking into account existing radial wave thermoacoustic theory and the common imperfections of nonuniform pore size and temperature discontinuities between the stack and heat exchangers. Swift briefly mentioned thermoacoustics in the radial mode of a cylindrical resonator,<sup>1</sup> and developed the radial mode thermoacoustic wave equation. Arnott *et al.* derived coupled first-order differential equations for pressure and specific acoustic impedance in a stack with a temperature gradient, and pressure and impedance translation equations for open resonator sections and heat exchangers.<sup>2</sup> Numerical implementation of these equations as described in Ref. 2 allows for the prediction of the onset temperature difference ( $\Delta T_{\text{onset}}$ ), the temperature difference across the stack at which acoustic oscillations are observed.

$\Delta T_{\text{onset}}$  is an important quantity in thermoacoustic engines for several reasons. The total power generated by a prime mover is the power generated by the stack (which is proportional to the temperature difference across the stack,  $\Delta T$ ) minus the thermal and viscous losses in the stack. A prime mover will begin to make sound when the total power generated in the stack overcomes other losses in the heat exchangers and the resonator.<sup>3,4</sup> Therefore,  $\Delta T_{\text{onset}}$  is proportional to the ratio of the acoustic power dissipated in the entire system (including the stack, heat exchangers, and any external load) to the acoustic power generated by the stack. Second, from an experimental vantage point,  $\Delta T_{\text{onset}}$  measurements are relatively easy to make, so that predictions and

measurements can be compared to determine the accuracy of the numerical model.

An outgrowth of this research was the need to elucidate experimental deviations from the theoretical ideal—a distribution of pore sizes within the stack rather than a uniform pore size and temperature discontinuities between the stack and the heat exchangers. Elementary methods of accounting for these complications are presented which bring experiment and theory into agreement.

## I. RADIAL WAVE THERMOACOUSTIC PRIME MOVER DESIGN

A schematic of the resonator portion of the radial thermoacoustic prime mover is shown in Fig. 1. The outer ring (A) is constructed of steel with inner and outer diameters of 148.6 cm and 156.2 cm. The top and bottom lids (B) have an outer diameter of 158.75 cm and a thickness of 2.54 cm. The center hole in B, for access to the thermoacoustic elements, has a diameter of 35.6 cm. All seals were made with o-rings. The caps (C) are constructed of stainless steel and have a groove cut at the location of the stack, leaving a  $\frac{1}{4}$ -in. plate over this region, to reduce thermal conduction of heat in the radial direction across the stack region of the resonator. When the caps (C) are placed into the holes in B, the inner faces of the caps are flush with the inner faces of the lids. The height of B, and thus the inner height of the resonator, is 10.2 cm. The assembled resonator has a mass of about 1360 kg. It should be noted that measures can be taken to significantly reduce the mass of the resonator.

The heat exchangers<sup>5</sup> are constructed of four standard  $\frac{1}{4}$ -in. copper tubes bent into circles, with copper plates (each

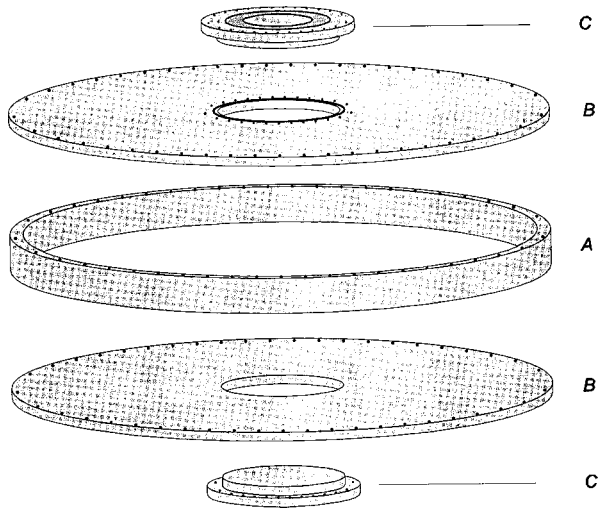


FIG. 1. Unassembled view of the resonator used for the large radial wave thermoacoustic prime mover. Pieces C are stainless steel caps which allow access to the inner thermoacoustic elements. Pieces A and B are plain carbon steel.

having four  $\frac{1}{4}$ -in. pre-punched holes to fit snugly over the tubing) fed onto the copper tubes. Steel washers were placed between the copper plates to maintain the correct spacing. The individual copper plates are 10 cm tall, 1.3 cm wide (radial dimension), and 0.76 mm thick. The washer spacers are also 0.76 mm thick, and the porosity or ratio of open area to total area of the heat exchangers is 0.32, where blockage by heat exchanger tubing and washer spacers has been taken into account. The inner (hot) heat exchanger was heated by dissipation of electrical current in 80% Nickel, 20% chromium wire inserted into the copper tubing and electrically insulated from the tubing with temperature resistant ceramic beads. The outer (cold) heat exchanger was cooled using tap water. The hot heat exchanger has an outer diameter of 23.8 cm and an inner diameter of 21.2 cm when fitted to the stack, while the cold heat exchanger has an outer diameter of 28.8 cm and an inner diameter of 26.3 cm when fitted to the stack.

The silicon bonded mica paper stack, with inner and outer diameters of 23.8 cm and 26.3 cm, was sandwiched between the two heat exchangers. The thickness of the individual stack pieces is 0.015 cm. Mica was chosen because of its high temperature tolerance (up to 773 K) and its low thermal conductivity of 0.163 W/(m\*K). The stack was formed by placing 183 of these pieces on top of each other with 8 smaller mica washers between each of the larger mica pieces to maintain the proper spacing. The spacer washers were 0.64 cm in diameter and 0.038 cm thick. The overall stack height was 10.2 cm. In an attempt to further maintain proper spacing in the stack, 0.015 cm diameter temperature resistant teflon thread was used between each pair of mica washer spacers to provide a total of 16 support locations equally spaced about the circumference of the stack.

A line drawing of the entire system is shown in Fig. 2. The Endevco 8510B microphone used for detection of the acoustic wave was located at a pressure antinode next to the outer wall of the resonator. It would be preferable to have the microphone at the center of the resonator, since the highest sound pressure levels (SPL) occur there, but high tempera-

tures precluded such a placement of the microphone. All other inlets to the resonator (i.e., plumbing, heating, gas valve, and thermocouples) are located at the pressure node in order to reduce losses due to any leaks at these junctures.

## II. MEASUREMENTS AND ASSOCIATED ERRORS

All temperature measurements were taken with type K thermocouples having a precision of  $\pm 1$  K. Test measurements with multiple thermocouples of the heat exchanger temperature varied by a maximum of 2 K, therefore temperature measurements were taken using a single thermocouple for each heat exchanger. The thermocouples were placed between plates of the heat exchangers and coupled to the heat exchangers using high temperature-high thermal conductivity paste. At  $\Delta T_{\text{onset}}$  the sound in the tube, initiated by a small tap on the resonator, increased instead of decaying. The error associated with the measurement of  $\Delta T_{\text{onset}}$  is estimated to be  $\pm 2$  K (the difference between the earliest  $\Delta T_{\text{onset}}$  after tapping and the  $\Delta T_{\text{onset}}$  obtained without tapping), so that the total error in temperature measurements is  $\pm 5$  K.

SPL was measured with an Endevco 8510B piezoresistive microphone which was calibrated using a piston-phonograph. The microphone output was routed to a dynamic signal analyzer for viewing the SPL as a function of frequency. The error associated with SPL measurements was less than 0.2 dB, and the frequency step size was 0.25 Hz.

## III. EXPERIMENTAL RESULTS AND COMPARISON TO THEORY

Several questions required measurements with the radial wave prime mover. The first had to do with theoretical predictions; can we predict the behavior of radial wave prime movers using radial wave thermoacoustic theory? The second was whether the radial modes reduce harmonic generation. Originally we were interested in the effect of sloped stacks in radial wave thermoacoustic engines, but theory has shown that the effect in radial prime movers with a natural slope between plates is minimal.<sup>6</sup>

### A. Initial comparison of experimental and theoretical onset temperatures

Measurements of  $\Delta T_{\text{onset}}$  have been made on the above described radial wave prime mover. Thermocouples were placed in the heat exchangers (attempts to measure the temperature at the face of the stack gave ambiguous results due to the short radial length of the stack and an inability to precisely position the thermocouple). Figures 3 and 4 show the lowest experimental  $\Delta T_{\text{onset}}$  results (solid circles) achieved as a function of ambient pressure, for air and argon, respectively. The ambient temperature in both cases was 293 K. Also shown are the theoretical predictions for the hot side temperature (dashed line) assuming that the stack faces maintain the same temperature as the heat exchangers. For the present discussion, the dotted lines in Figs. 3 and 4 should be ignored. It is obvious that theory and experiment

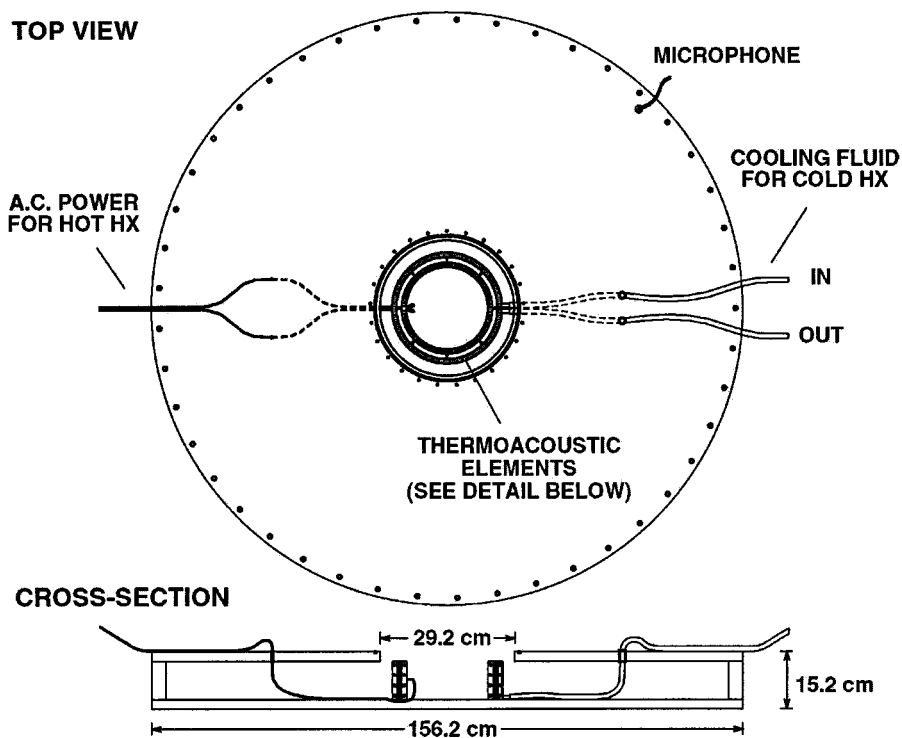
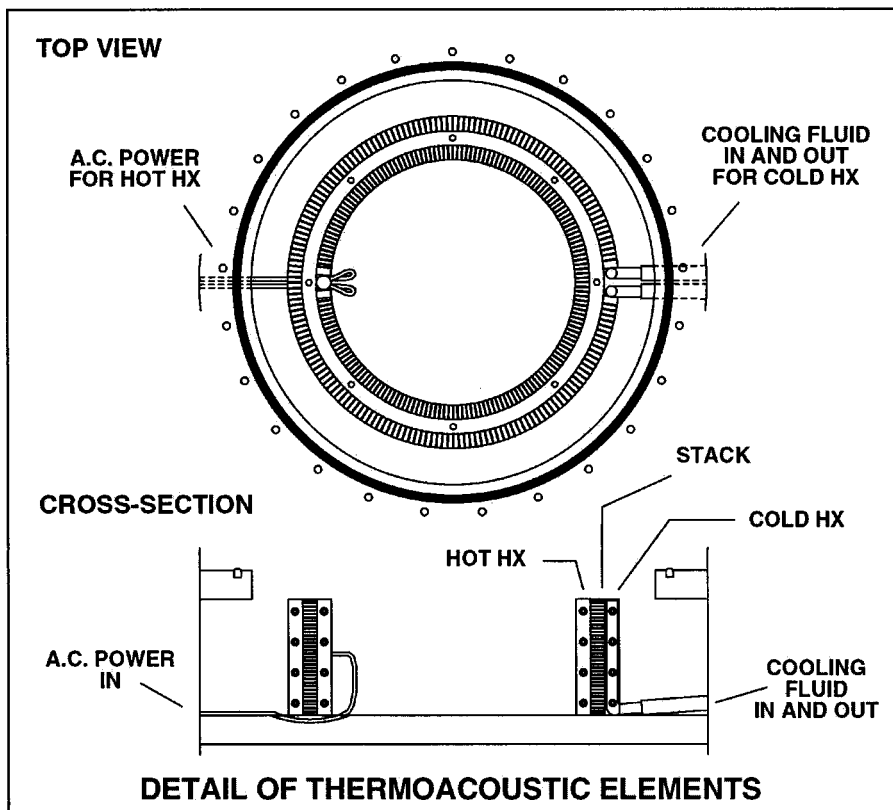


FIG. 2. Line drawing of the radial wave thermoacoustic prime mover.



are not at all in agreement, with the experimental onset temperatures being significantly higher than predicted for both gases.

There are several complicating features of our radial engine. First, for computations the stack was assumed to have a fixed pore size or plate spacing, but measurements show that a distribution of pore sizes exists. Second,  $\Delta T_{\text{onset}}$  is sensitive to the "fit" of the heat exchangers around the stack, a fact which is enhanced by the short radial length of the stack

as will be shown later. The heat exchanger "fit" is not as difficult in the plane wave case, since the manufacture of a flat heat exchanger surface is easily achieved so that the stack surfaces can be flush against heat exchangers with no alteration of the stack pore shape, so that direct thermal contact is sustained between the stack and the heat exchanger. Such a fit is more difficult in the radial case since the heat exchanger surfaces must maintain perfect curvature to provide the best possible thermal contact between stack and heat

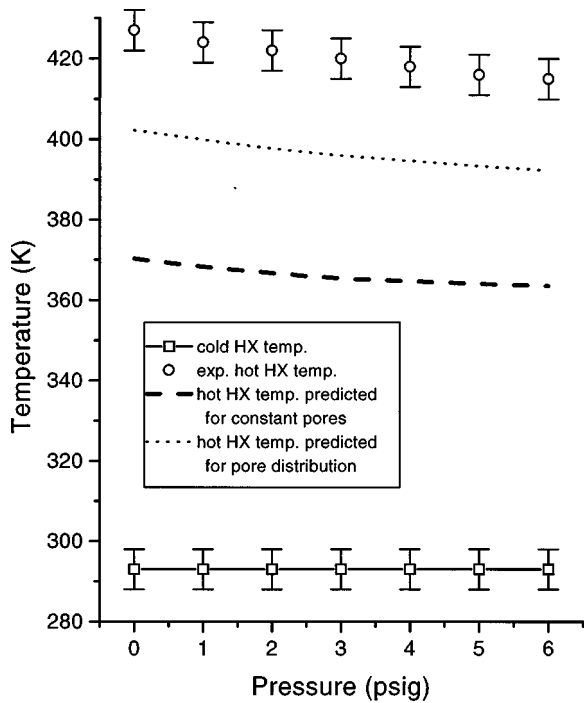


FIG. 3. Onset temperatures for the radial wave prime mover with air as the working fluid, assuming no temperature discontinuity between the stack and heat exchangers. Solid line shows cold heat exchanger temperature; dashed line is the predicted hot heat exchanger temperature for a stack with a single pore size; dotted line is the predicted hot heat exchanger temperature for the stack with the pore distribution shown in Fig. 5; and circles show experimental results.

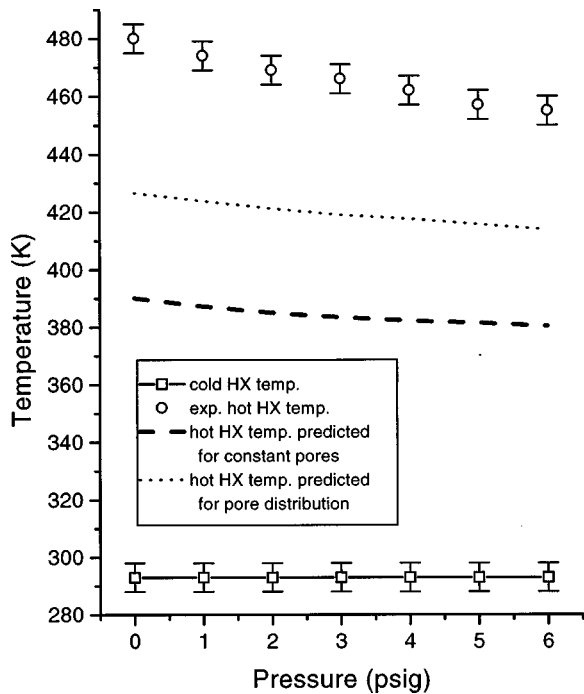


FIG. 4. Onset temperatures for the radial wave prime mover with argon as the working fluid, assuming no temperature discontinuity between the stack and heat exchangers. Solid line shows cold heat exchanger temperature; dashed line is the predicted hot heat exchanger temperature for a stack with a single pore size; dotted line is the predicted hot heat exchanger temperature for the stack with the pore distribution shown in Fig. 5; and circles show experimental results.

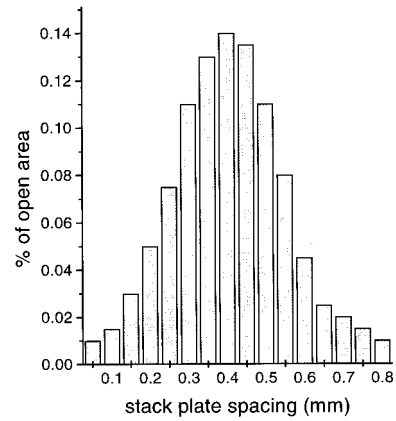


FIG. 5. Area distribution of plate spacing in the radial prime mover stack.

exchanger. Attempts to force the heat exchangers against the stack, thus creating the necessary curvature in the heat exchangers, tend to distort the stack plate spacing. Since the heat exchanger is much more rugged than the stack, a point is reached where the stack conforms to the heat exchanger shape via warping of the stack plates rather than the heat exchanger conforming to the stack shape. For identical gas compositions and pressures, results for  $\Delta T_{\text{onset}}$  varied depending upon the proximity of the heat exchangers to the stack and the stack distortion.

## B. Nonuniform stack plate spacing

As mentioned previously, attempts were made to maintain a constant plate spacing throughout the stack by using mica washer spacers and later by adding teflon thread to maintain the correct spacing. In hindsight, it would have been much better to use thicker (and thus more rigid) mica plates in the stack at the expense of reducing the stack porosity (this would also have prevented additional distortion of the stack spacing due to pressure from the heat exchangers). In order to characterize the present stack, measurements of the plate spacing were taken over the entire height of the stack, assuring that the average spacing is equal to the originally expected constant spacing. Radial variations in plate spacing were negligible. Over 500 measurements were made to ensure an accurate representation of the axial/azimuthal pore size distribution. The measurements were by necessity taken without the heat exchangers in place, such that no plate warping was introduced by pressure from the heat exchangers. Ideally, measurements would have been repeated with the heat exchangers in place. However, since  $\Delta T_{\text{onset}}$  measurements in the following sections were taken for cases in which the heat exchangers were pressed as tightly as possible against the stack *without* distorting it, pore measurements of the stack alone should be sufficient. Figure 5 shows the measured distribution in terms of the percent of the total open area in the stack occupied by each gap size.

Prediction of  $\Delta T_{\text{onset}}$  for a stack with a distribution of pore sizes is accomplished by treating the various pore sizes as having parallel impedances. The electrical analog would be parallel resistors. Beginning with a known impedance and pressure amplitude at the hot, rigid end of the resonator, the

pressure and impedance at the hot face of the stack may be determined using translation theorems, Eqs. (5) and (6) of Ref. 2. The boundary conditions at the hot face of the stack are continuity of pressure and volume velocity, so

$$P_{1j} = P_H, \quad (1)$$

and

$$\sum_j A_j V_{1j} = A_H V_H, \quad (2)$$

where  $j$  represents quantities for a particular pore size, subscript 1 denotes that the quantity is evaluated at the hot end of the stack,  $P_{1j}$  is the complex acoustic pressure at the hot side of an individual pore,  $P_H$  is the pressure at the hot face of the stack determined by translation,  $A_j$  is the stack cross-section occupied by a particular pore size,  $A_H$  is the resonator cross-sectional area at the hot face of the stack,  $V_{1j}$  is the bulk particle velocity averaged over the cross-section of the stack having a given plate spacing at the hot side, and  $V_H$  is the velocity at the hot face of the stack determined by translation.

To obtain a full numerical solution to the problem, it would be necessary to guess the complex pressure  $P_C$  and the various pore velocities at the cold side of the stack, integrate backward to the hot side of the stack checking to see if the conditions in Eqs. (1) and (2) had been met, and repeat the process with new guesses until the solution converged. This would require scanning an extremely large parameter space. Therefore, the method of Raspet *et al.* for approximating thermoacoustic calculations using a single step<sup>7</sup> has been utilized to reduce computation times. The single step method was shown to be accurate for  $|kL| \leq 0.3$ , where  $L$  is the stack length and  $k$  is the wave number. The radial prime mover certainly meets this criterion since  $|kL| \approx 0.065$ .

Assumptions are that the acoustic pressure is constant across the pore cross section and is a function only of the radial distance along the pore, and that the transverse velocity is small relative to the radial velocity. The relevant equations describing the fluid motion in the pore are taken from Eqs. (7) and (8) of Ref. 2 [with porosity accounted for such that  $v_r(r) = V_j/\Omega_j$ , where  $\Omega_j$  is the porosity for a given pore size and  $V_j = P_j/Z_j$ ] and are given by

$$V_j = \frac{\Omega_j F_j(\lambda_j)}{i\omega\rho_0} \frac{dP_j}{dr} \quad (3)$$

and

$$\frac{dV_j}{dr} + \frac{1}{T} \frac{dT}{dr} \left[ \frac{F_j(\lambda_{Tj})/F_j(\lambda_j) - 1}{1 - N_{Pr}} \right] V_j + \frac{V_j}{r} + \frac{\Omega_j F_j(\lambda_j)}{i\omega\rho_0} k_j^2 P_j = 0, \quad (4)$$

where  $k_j^2$  is given by Eq. (4) of Ref. 2. The finite difference forms of these equations are given by

$$iC_j \frac{V_{1j} + V_{2j}}{2} = \frac{P_{1j} - P_{2j}}{L} \quad (5)$$

and

$$iC_j \frac{V_{1j} - V_{2j}}{L} + iC_j D_j \frac{V_{1j} + V_{2j}}{2} + k_j^2 \frac{P_{1j} + P_{2j}}{2} = 0, \quad (6)$$

where

$$C_j = \frac{\omega\rho_0}{\Omega_j F_j(\lambda_j)}, \quad (7)$$

and

$$D_j = \frac{1}{T} \frac{dT}{dr} \left[ \frac{F(\lambda_{Tj})/F(\lambda_j) - 1}{1 - N_{Pr}} \right] + \frac{1}{r}. \quad (8)$$

The subscript 2 refers to pore quantities at the cold side of the stack, subscript 1 to pore quantities at the hot side of the stack, subscript  $j$  to pores of a particular size, and all parameters are evaluated at the center of the stack. Note that the volume coefficient of expansion,  $\beta$ , in Eq. (8) has been replaced by the ideal gas result,  $1/T$ .<sup>8</sup> Equations (5) and (6) may be combined to eliminate  $V_{2j}$  so we are left with  $V_{1j}$  in terms of  $P_{1j}$  and  $P_{2j}$

$$V_{1j} = \frac{1}{iC_j L} \left\{ P_{1j} \left[ 1 - \frac{D_j L}{2} - \frac{k_j^2 L^2}{4} \right] - P_{2j} \left[ 1 - \frac{D_j L}{2} + \frac{k_j^2 L^2}{4} \right] \right\}. \quad (9)$$

Now we need only to guess the magnitude and phase of  $P_{2j}$ , and use the known pressure  $P_{1j}$  to determine  $V_{1j}$ . These values of  $V_{1j}$  are then tested to see if the condition in Eq. (2) holds. If the requirement is not met,  $P_{2j}$  is adjusted and the process is repeated. When the requirement is met, Eq. (5) is rearranged to give  $V_{2j}$  using the now known values for  $V_{1j}$ ,  $P_{1j}$ , and  $P_{2j}$ . The pressure and velocity at the cold side of the stack are then determined by requiring conservation of pressure and volume velocity

$$P_C = P_{2j} \quad (10)$$

and

$$A_C V_C = \sum_j A_j V_{2j}, \quad (11)$$

where  $P_C$  is the pressure in the tube at the cold face of the stack,  $A_C$  is the resonator cross-section at the cold face of the stack, and  $V_C$  is the area averaged particle velocity in the tube at the cold face of the stack.

Using the method outlined above,  $\Delta T_{\text{onset}}$  was determined for a stack having a distribution of pore sizes. The dotted lines in Figs. 3 and 4 show corrections, using the measured pore distribution of Fig. 5, to the constant pore size results represented by dashed lines for the hot side temperature at onset in air and argon, respectively. Physically, the reason for the increased  $\Delta T_{\text{onset}}$  as a result of the pore distribution is due to the fact that only the pore spacings in the middle of the distribution have the correct ratio of penetration depth to pore size, while the pores with other sizes are not acting as efficiently. It is obvious that the pore distribution in the stack explains a significant portion of the discrepancy between experiment and theory, but further interpretation is required to account for the remaining disparity.

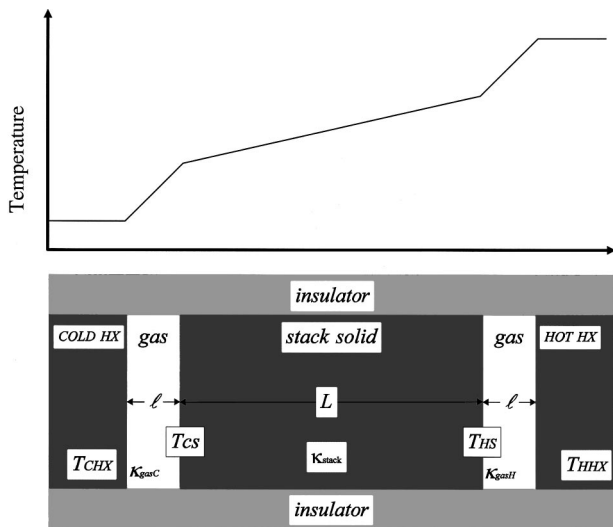


FIG. 6. Illustration of the gaps present between the radial stack and heat exchangers. The upper plot shows a representative temperature distribution over the heat exchanger-gap-stack-gap-heat exchanger system. Temperature is constant in the heat exchangers, while the gradient is larger in the gaps than in the stack.

### C. Temperature discontinuities between the heat exchanger and the stack face

As the stack in a thermoacoustic prime mover becomes very short, the temperature gradient necessary for onset of oscillations increases, which in turn raises the amount of heat flowing via thermal conduction from the hot side to the cold side of the stack. In addition, any small gap between the stack and the heat exchanger becomes a more appreciable percentage of the stack length, so that heat which is conducted across the gap may no longer be ignored by assuming that the stack face and the heat exchanger maintain the same temperature. Rather, it becomes necessary to account for conduction through the fluid across gaps between the stack and heat exchanger as well as for normal thermal conduction through the stack, when determining the temperatures at the faces of the stack which ultimately cause onset.

A simple model may be used to explain the remaining difference between experiment and theory, and why the difference is much more noticeable for the radial engine than for a plane wave device. Consider the heat exchanger-stack-heat exchanger pictured in Fig. 6. Perfect insulators have been placed on top and bottom to confine heat flows to the horizontal direction. The hot and cold heat exchangers are held at temperatures  $T_{HHX}$  and  $T_{CHX}$ . Rather than assuming that the stack face and the heat exchanger are in physical contact and at the same temperature, they are separated by a small gap of length  $\ell$  filled with gas. The stack length is denoted by  $L$ . Assumptions are: heat is transported only by conduction,  $\kappa_C$  (the thermal conductivity of the gas in the gap near the cold heat exchanger) is evaluated at a temperature of  $T_{CHX}$ ,  $\kappa_H$  (the thermal conductivity of the gas in the gap near the hot heat exchanger) is evaluated at a temperature of  $T_{HHX}$ ,  $\kappa_S$  (the thermal conductivity of the solid stack material) is assumed to be constant and is evaluated at a temperature of  $\frac{1}{2}(T_{HHX} + T_{CHX})$ . Our goal is to find the hot and cold side stack temperatures,  $T_{HS}$  and  $T_{CS}$ , in terms of

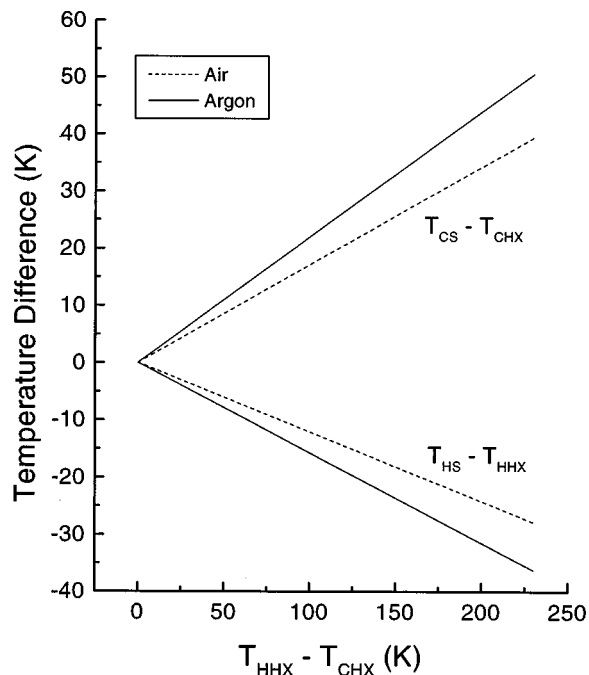


FIG. 7. Demonstration of the temperature discontinuity between the stack and heat exchanger face for  $\ell/L = 0.036$ . The various temperature locations are shown pictorially in Fig. 6.

the known quantities  $\ell$ ,  $L$ ,  $T_{CHX}$ ,  $T_{HHX}$ ,  $\kappa_C$ ,  $\kappa_H$ , and  $\kappa_S$ . Assuming linear temperature gradients within the three regions and requiring heat flow to be continuous at all boundaries, application of the 1D steady state heat equation yields

$$T_{HS} = \frac{\kappa_H T_{HHX} + \kappa_C T_{CHX} \kappa_C T_{CS}}{\kappa_H} \quad (12)$$

and

$$T_{CS} = \frac{[\kappa_C \kappa_H + \kappa_C \kappa_S (\ell/L)] T_{CHX} + \kappa_H \kappa_S T_{HHX} (\ell/L)}{\kappa_H \kappa_C + \kappa_H \kappa_S (\ell/L) + \kappa_C \kappa_S (\ell/L)} \quad (13)$$

Examining Eqs. (12) and (13), it is evident that as  $\ell/L \rightarrow 0$ ,  $T_{HS} \rightarrow T_{HHX}$  and  $T_{CS} \rightarrow T_{CHX}$  as expected. In the case of the radial wave prime mover,  $L = 1.25$  cm and a good average estimate for  $\ell$  (determined by physical measurement of the gaps between the heat exchangers and the stack) is  $\ell = 0.45$  mm, producing a ratio of  $\ell/L = 0.036$ . For the typical 5.08 cm plane wave stack of Ref. 9, a conservative estimate would be  $\ell = 0.025$  mm so that  $\ell/L = 0.002$ .

Figures 7 and 8 show deviations of the stack face temperatures from the heat exchanger temperatures over a range of heat exchanger temperature differences for the above values of  $\ell/L$  for air and argon. From these figures we see that the radial prime mover does a poor job of establishing the expected temperature difference across the stack due to the short radial length of the stack and the presence of non-negligible gaps between the stack and heat exchanger. For a 150 K difference across the heat exchangers, the actual difference across the stack is only 106 K for air and 94 K for argon, while a conservative estimate for the 5.08 cm stack of Ref. 9 gives differences of 147 K for air and 144 K for

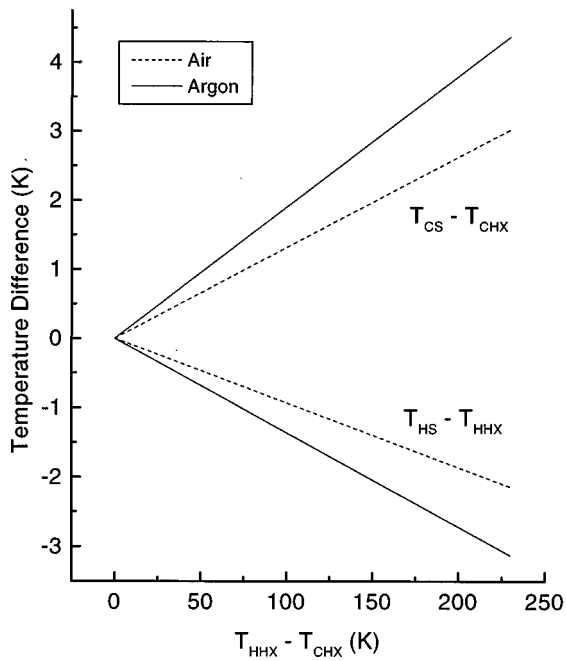


FIG. 8. Demonstration of the temperature discontinuity between the stack and heat exchanger face for  $\ell/L=0.002$ . The various temperature locations are shown pictorially in Fig. 6.

argon. These results indicate that assuming the heat exchanger temperature was equivalent to the stack face temperature was not appropriate.

Previously, it was mentioned that experimental measurements of  $\Delta T$  varied depending upon the “fit” of the heat exchangers to the stack. Measurements of the gap between the heat exchangers and the stack range from 0 to 0.6 mm when the heat exchangers are tightened and pressed against the stack. The upper end of this range can be reduced to about 0.4 mm by lightly hammering the heat exchanger against the stack. Measurements have been made for a forced (hammered) and an unforced (only tightened and pressed) fit of the heat exchangers against the stack. In both cases,  $\ell$  should be close to the average measured gap value, although a slight variance due to azimuthal heat flows in the fluid and the stack may do a better job of modeling the experimental results. Therefore, an effective gap length,  $\ell_{\text{eff}}$ , is defined to simulate the effect that the entire gap distribution has on  $\Delta T_{\text{onset}}$ .

In order to compare experiment with theory using the measured distribution of pore sizes and accounting for a gap between the stack and heat exchangers,  $T_{\text{CS}}$  and  $T_{\text{HS}}$  are calculated using the measured values for  $T_{\text{CHX}}$  and  $T_{\text{HHX}}$  for a guessed  $\ell_{\text{eff}}$  in air, the initial guess being the average measured gap size.  $T_{\text{CS}}$  is then used as the cold side stack temperature in the  $\Delta T_{\text{onset}}$  calculation to determine the predicted hot side temperature required for onset, denoted by  $T_{\text{HS calc}}$ . This predicted value is compared with  $T_{\text{HS}}$ .  $\ell_{\text{eff}}$  is then adjusted and the process repeated until  $T_{\text{HS calc}}$  and  $T_{\text{HS}}$  best match up over a range of pressures. Admittedly, this process is backward, since  $\ell_{\text{eff}}$  is adjusted to give the best possible results for a given gas (air). However, if the theory is correct, then the resulting  $\ell_{\text{eff}}$  for one gas should be applicable to other gases as well. Therefore, the  $\ell_{\text{eff}}$  determined for air is

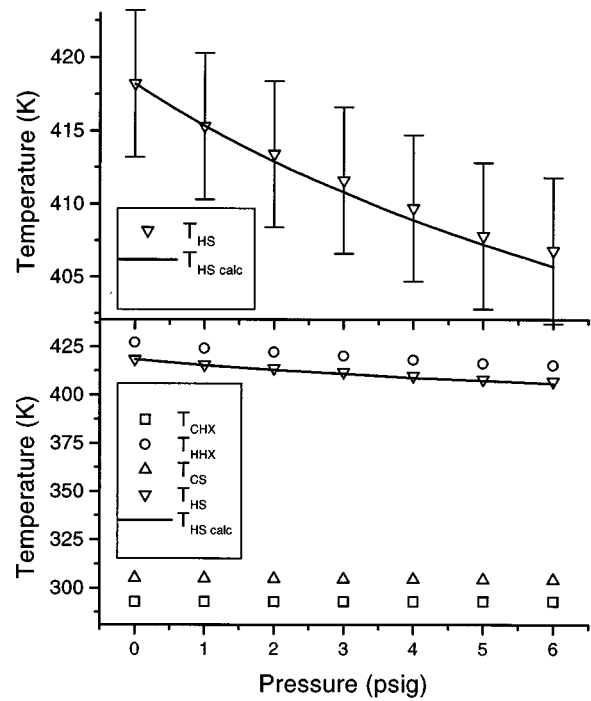


FIG. 9. Air results for  $\ell_{\text{eff}}=0.2$  mm. The upper plot is a blown up version of  $T_{\text{HS}}$  and  $T_{\text{HS calc}}$  in the lower plot, where  $T_{\text{HS calc}}$  is the numerically predicted onset temperature using  $T_{\text{CS}}$  as the temperature at the cold side of the stack. Measured temperatures are represented by circles and squares, while triangles represent calculations. Errors in the lower plot are smaller than the data points.

used to determine  $T_{\text{CS}}$  and  $T_{\text{HS}}$  for the prime mover filled with argon, and the resulting  $T_{\text{HS}}$  is compared with  $T_{\text{HS calc}}$  for argon.

Figures 9 and 10 show  $T_{\text{CHX}}$ ,  $T_{\text{CS}}$ ,  $T_{\text{HS}}$ ,  $T_{\text{HHX}}$ , and  $T_{\text{HS calc}}$  for air and argon, respectively. Note that measured temperatures are represented by the squares and circles, while triangles represent calculated values. The experimental results are the same as those shown in Figs. 3 and 4, and again represent the configuration giving the lowest  $\Delta T_{\text{onset}}$ . Keep in mind that  $T_{\text{CHX}}$  and  $T_{\text{HHX}}$  are experimental results, however, the comparison will be between the calculated-from-experiment  $T_{\text{HS}}$  and the predicted hot side stack temperature  $T_{\text{HS calc}}$ . In the upper plot of Fig. 9, we see that a chosen value of  $\ell_{\text{eff}}=0.2$  mm produces nice agreement for air. Applying this value of  $\ell_{\text{eff}}$  to the argon data, we see in the upper plot of Fig. 10 that  $T_{\text{HS}}$  and  $T_{\text{HS calc}}$  are within 5 K of each other over the pressure range tested, and appear to be following the same general trend. It should be mentioned at this point that it would have been nice to extend the pressure range over which measurements were made, however, due to the large flat surface area of the resonator, increasing the pressure beyond 6 psig would have placed an exorbitant amount of force upon the bolts holding the resonator together, and could have caused the steel plates to bow outward.

Measurements were also made which gave higher onset temperatures due to a looser fitting of the heat exchangers. Figures 11 and 12 show the results for air and argon, respectively.  $\ell_{\text{eff}}=0.41$  mm provides good agreement between  $T_{\text{HS}}$  and  $T_{\text{HS calc}}$  in air. Applying this  $\ell_{\text{eff}}$  to the argon data also

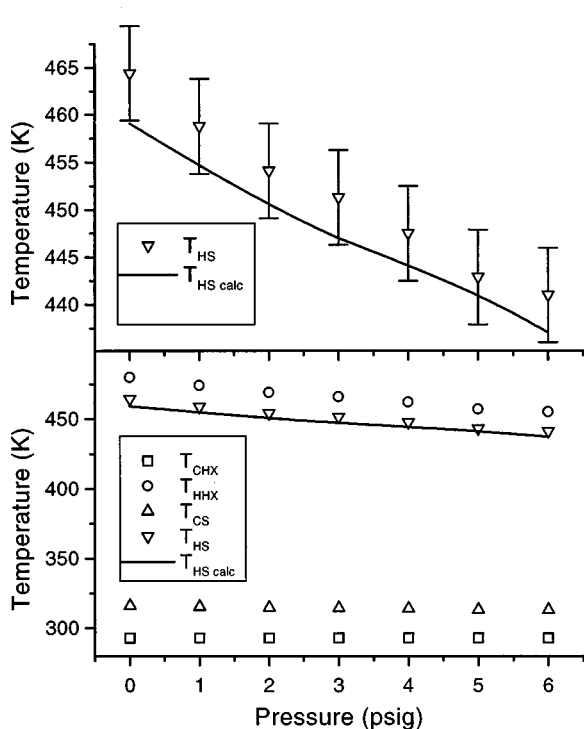


FIG. 10. Argon results for  $\ell_{\text{eff}}=0.2$  mm. The upper plot is a blown up version of  $T_{\text{HS}}$  and  $T_{\text{HS calc}}$  in the lower plot, where  $T_{\text{HS calc}}$  is the numerically predicted onset temperature using  $T_{\text{CS}}$  as the temperature at the cold side of the stack. Measured temperatures are represented by circles and squares, while triangles represent calculations. Errors in the lower plot are smaller than the data points.

gives good results, such that  $T_{\text{HS}}$  and  $T_{\text{HS calc}}$  are within 8 K of each other, and again the general trend of the curves are the same. The agreement is not as good as in the previous case, due to a larger distribution of gaps between the stack and heat exchangers. In particular, we have assumed that  $\ell_{\text{eff}}$  is the same at the hot and cold sides of the stack. For a looser fit of the heat exchangers on the stack, this assumption becomes less valid than in the case where the heat exchangers were fit as tightly as possible *without disfiguring the stack*.

#### D. Radial prime mover harmonic generation

In most cases, the linear acoustic wave equation suffices to describe the behavior of a system. However, when the acoustic pressure amplitude becomes large, higher order terms must be taken into account. Coppens and Sanders accounted for nonlinear effects for finite-amplitude standing waves in a resonance tube by modifying the linear equations of state and continuity to allow for second-order effects.<sup>10</sup> Chen included an additional second-order term in the momentum equation for the same problem and found the correction to be small,<sup>11</sup> as would be expected since good agreement was shown between theory and experiment using the Coppens and Sanders approximation.

The general behavior of a prime mover was effectively described by Atchley *et al.*<sup>12</sup>

“Once onset of self oscillation is reached, the acoustic amplitude in the tube immediately assumes a large value, typically about 1% of the ambient pressure. The observed waveform is noticeably nonsinu-

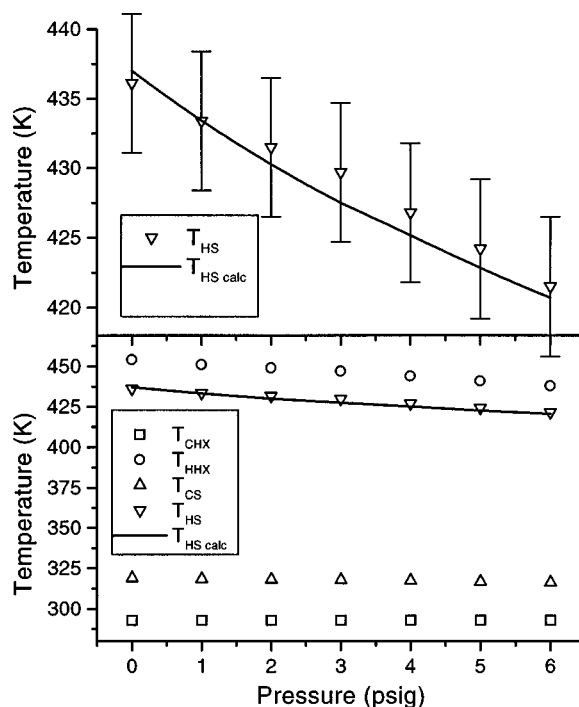


FIG. 11. Air results for  $\ell_{\text{eff}}=0.41$  mm. The upper plot is a blown up version of  $T_{\text{HS}}$  and  $T_{\text{HS calc}}$  in the lower plot, where  $T_{\text{HS calc}}$  is the numerically predicted onset temperature using  $T_{\text{CS}}$  as the temperature at the cold side of the stack. Measured temperatures are represented by circles and squares, while triangles represent calculations. Errors in the lower plot are smaller than the data points.

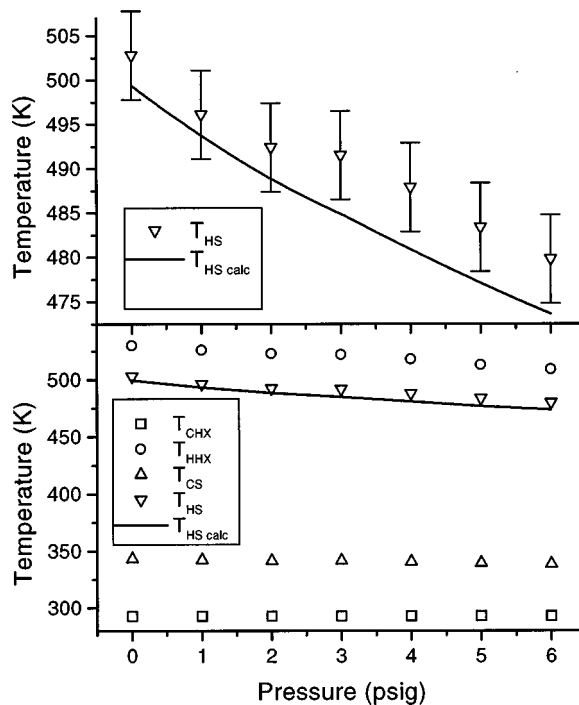


FIG. 12. Argon results for  $\ell_{\text{eff}}=0.41$  mm. The upper plot is a blown up version of  $T_{\text{HS}}$  and  $T_{\text{HS calc}}$  in the lower plot, where  $T_{\text{HS calc}}$  is the numerically predicted onset temperature using  $T_{\text{CS}}$  as the temperature at the cold side of the stack. Measured temperatures are represented by circles and squares, while triangles represent calculations. Errors in the lower plot are smaller than the data points.

soidal. As more energy is supplied to the hot end of the stack, the temperature of that end increases only slightly while the acoustic amplitude in the tube increases rapidly... Unfortunately, as the acoustic amplitude increases, an increasing fraction of the acoustic energy appears as higher harmonics—harmonic distortion increases.’’

The authors presented results for a constant cross-section plane wave prime mover immediately after onset and also when the hot end temperature was raised 43 K beyond the necessary temperature for onset. In both cases, nonlinear generation of higher harmonics was demonstrated. The experimental results for the relative amplitudes of the harmonics to the fundamental in the prime mover just beyond onset provided nice agreement with the theory of Ref. 10.

It is desirable in a prime mover to minimize the generation of higher harmonics so that more acoustic energy is channeled into the fundamental. In a plane wave resonator, one of the ways to accomplish this is to vary the cross-section of the tube.<sup>13</sup> This detuning causes the natural modes of the resonator to be anharmonic. Gaitan and Atchley,<sup>14</sup> following the method outlined by Coppens and Sanders<sup>15</sup> in a later paper, investigated higher harmonic generation in tubes with harmonic and anharmonic natural modes for application to thermoacoustic engines. The anharmonic tubes were made by varying the cross-section in the center of the tube to a size different than at the ends. Experimental results for the amplitudes of the harmonics for a given amplitude of the fundamental were in excellent agreement with theory for both tube types. In the case of the harmonic tube, the amplitude of the first harmonic was only 10–20 dB below the fundamental, depending upon the acoustic pressure amplitude of the fundamental. However, in two separate anharmonic tubes (one with a larger center cross-section than at the ends and one with a smaller center cross-section) the amplitude of the first harmonic was reduced 30–40 dB below the fundamental.

The generic nonlinear wave equation presented in Ref. 1 is

$$\sum_n \left( c_n^2 \nabla^2 - \frac{\partial^2}{\partial t^2} + \frac{n\omega}{Q_n} \frac{\partial}{\partial t} \right) \frac{p_n}{\rho_0 c^2} \doteq - \frac{\partial^2}{\partial t^2} \left[ \left( \frac{u}{c} \right)^2 + \frac{\gamma-1}{2} \left( \frac{p}{\rho_0 c^2} \right)^2 \right], \quad (14)$$

where  $c_n$  and  $Q_n$  are the sound speed and quality factor of the  $n$ th resonance of the tube,  $\omega$  is the angular driving frequency (the fundamental resonance for a prime mover),  $p_n$  is the acoustic pressure of the  $n$ th harmonic of the driving frequency,  $u$  and  $p$  are the total acoustic velocity and pressure and are functions of radial location  $r$  in radial systems (or longitudinal position  $z$  in plane systems) and time  $t$ . Equation (18) is valid near resonance and assumes the total standing wave to be of the form

$$p = \sum_{n=1}^{\infty} p_n = \sum \rho_0 c^2 M R_n \cos(nkz) \sin(n\omega t + \phi_n), \quad (15)$$

where  $M$  is the peak Mach number of the fundamental,  $R_n$  is the nondimensional amplitude of the  $n$ th harmonic,  $k$  is the wave number of the driving frequency, and  $\phi_n$  is the temporal phase of the  $n$ th harmonic. For a radial system, Eq. (15) would have  $J_0$  in place of cosine. The harmonic amplitudes,  $R_n$ , are shown in Refs. 14 and 15 to be directly proportional to

$$R_n \propto Q_n \cos \left( \tan^{-1} \left( 2Q_n \frac{n\omega\omega_n}{\omega_n} \right) \right), \quad (16)$$

where  $\omega_n$  denotes normal modes of the resonator, so that the harmonic amplitudes are maximized when the normal modes correspond exactly to the harmonics of the fundamental frequency. Therefore, a detuned resonator leads to a reduction in the amplitudes of the harmonics.

With the existing radial wave prime mover, we are limited to examination of the behavior of the system just above onset. The reason for this is that when attempts are made to increase the temperature beyond onset, the following cycle ensues. When the necessary temperature difference is reached, sound is produced. The system responds with an increased acoustic pressure amplitude and thus increased acoustic heat transport from the hot side to the cold side of the stack. The cold heat exchanger, unable to sustain its temperature with the increased heat load, begins to heat up such that the temperature difference across the stack falls below the necessary difference for oscillations to be maintained. When the acoustic wave ceases, the acoustic heat transport also ceases, and the cold heat exchanger returns to its original cooler temperature. Once again the temperature difference reaches the critical onset value, the acoustic wave is regenerated, and the cycle is repeated. A similar effect was observed by Olson and Swift in a plane wave prime mover.<sup>16</sup> Although it would be nice to get a comparison of plane and radial prime movers at lower and higher acoustic pressure amplitudes, the results for temperatures just above onset should give some insight into the reduction of higher harmonic generation which occurs in radial systems as compared to constant cross-section plane systems.

Figure 13 shows a spectrum from the previously described radial wave prime mover. The hot heat exchanger temperature is 427 K and the ambient heat exchanger temperature is 293 K, giving a temperature difference of 134 K. The fundamental frequency of oscillation is 288 Hz in air at atmospheric pressure. The sound pressure level (SPL) at the microphone is 153 dB. The SPL at the center of the resonator is estimated to be 161 dB. The first radial wave harmonic occurs at 526 Hz, but there is no noticeable signal at this frequency. The first nonlinear harmonic occurs at twice the fundamental, or 584 Hz. There is a significant harmonic generation at this frequency, with an SPL of 115 dB. However, this is 38 dB below the fundamental. These results are very similar to those of Ref. 14 for a detuned plane wave resonator driven by a piston. In both cases, the first harmonic is nearly 40 dB below that of the fundamental, and there is no noticeable sound production at the other normal modes of the tubes. In the radial prime mover, the second and third nonlinear harmonics occur at three and four times the fundamen-

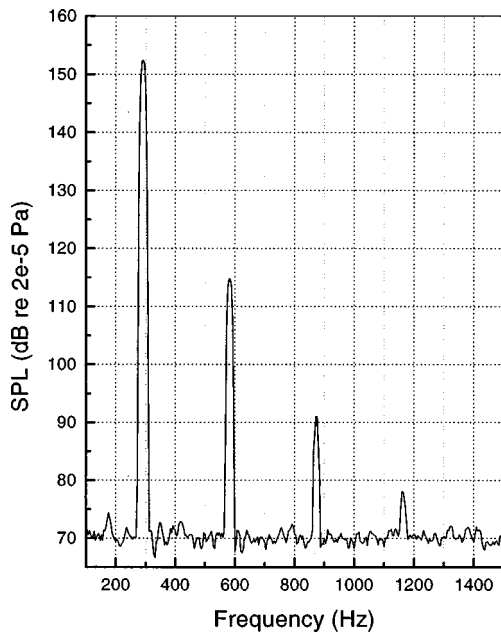


FIG. 13. Acoustic spectrum from the radial wave prime mover in air at atmospheric pressure.

tal, 876 Hz and 1.168 kHz, and are 63 dB and 75 dB below the fundamental, respectively.

For comparison, a constant cross-section plane wave prime mover was constructed and the spectrum is shown in Fig. 14. A schematic of the prime mover, which is similar in design to that described by Belcher,<sup>9</sup> is shown in Fig. 15. The hot heat exchanger temperature was 410 K and the ambient heat exchanger temperature was 300 K for a temperature difference of 110 K. The frequency of operation was the same as in the radial case, 288 Hz, and the thermoacoustic elements were located at the position predicted to give the lowest temperature difference necessary to produce sound. A ceramic square pore stack and parallel-plate copper heat exchangers were used. The microphone was located at the am-

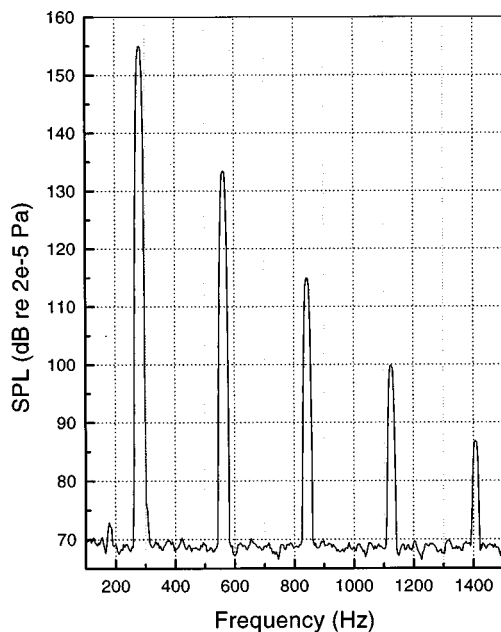


FIG. 14. Acoustic spectrum from the plane wave prime mover in air at atmospheric pressure.

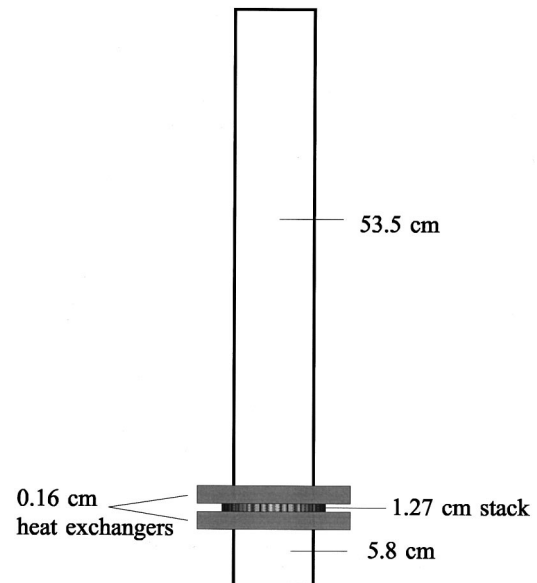


FIG. 15. Plane wave model with dimensions similar to the proposed large radial wave thermoacoustic prime mover. All lengths shown are in the vertical direction. The tube diameter is 8.5 cm.

bient end of the tube. The sound pressure level (SPL) at the microphone was 156 dB. The first harmonic occurs at twice the fundamental frequency, or 576 Hz. There is a large contribution at this frequency, with an SPL of 137 dB, only 19 dB below the fundamental (compared to a first harmonic which was 38 dB below the fundamental in the radial prime mover). The first through sixth harmonics give noticeable contributions in the plane engine compared to only the first through third harmonics in the radial engine. The results of the plane wave prime mover are similar to those of Ref. 12 for a prime mover just beyond onset, and Ref. 14 for a harmonic resonator driven by a piston. In all three cases, the first harmonic has an amplitude about 20 dB below the fundamental with more harmonics having significant amplitudes than in the radial and detuned plane resonators.

The reduction in higher harmonic generation for the radial engine is understood qualitatively by considering the proximity of the nonlinear higher harmonics to the natural modes or overtones of the resonator. In general, the nonlinear harmonics have a very narrow bandwidth<sup>12</sup> while the overtones have a wider bandwidth. In the case of the plane resonator the nonlinear harmonics are not exactly the same as the overtones, since a very slight detuning of the overtones occurs due to dissipation in the resonator and the thermoacoustic elements; however, the two are in the same vicinity so that the nonlinear harmonics certainly fall within the bandwidth of the overtones, thus enhancing the higher harmonic generation. The radial engine and detuned plane resonators, by contrast, have no overtones in the vicinity of the nonlinear harmonics so that these systems do not enhance the generation of higher harmonics. A convenience of a radial system is that no variation in tube shape is necessary to make the resonator anharmonic.

#### IV. CONCLUSIONS

The primary goal of this research was to test the radial wave thermoacoustic theory. Although some satisfaction is

lost in not being able to directly compare measured onset temperatures with predicted values due to unforeseen physical constraints on the system (i.e., significant gaps between stack and heat exchanger), with these constraints included, it has been shown that the existing radial wave theory is accurate and useful for prediction of engine performance.

A secondary goal was to test the generation of higher harmonics in a radial mode prime mover. The expected result was attained. Comparison of harmonic generation in the radial prime mover and a similar plane prime mover showed that the radial prime mover does not enhance the generation of higher harmonics, since the resonator harmonics are not in the vicinity of multiples of the fundamental. In addition, sound pressure levels of the higher harmonics in the radial prime mover were found to be similar to those produced by a detuned plane prime mover.

We identified several areas in which care should be taken in future research, and developed some useful tools for understanding these problem areas. In radial engines, stack plates which are rigid enough to provide a constant plate spacing should be used. Since the radial stack was characterized by a distribution of pore sizes rather than a constant pore size, a method was developed for analyzing pore distributions in the stack. This should be a useful first step in the analysis of inhomogeneous stacks (i.e., steel wool, fiberglass, etc.). In addition, some difficulties with short stacks have been discovered and understood. It was shown that the fit of the heat exchanger to the stack is much more important when short stacks are used.

#### ACKNOWLEDGMENT

The authors wish to gratefully acknowledge the support of the Office of Naval Research.

- <sup>1</sup>G. W. Swift, "Thermoacoustic engines," *J. Acoust. Soc. Am.* **84**, 1145–1180 (1988).
- <sup>2</sup>W. P. Arnott, J. A. Lightfoot, R. Raspet, and Hans Moosmüller, "Radial wave thermoacoustic engines: Theory and examples for refrigerators and high-gain narrow-bandwidth photoacoustic spectrometers," *J. Acoust. Soc. Am.* **99**, 734–745 (1996).
- <sup>3</sup>J. Wheatley, "Intrinsically irreversible or natural engines," in *Frontiers in Physical Acoustics* (Elsevier, New York, 1986).
- <sup>4</sup>W. P. Arnott, J. R. Belcher, R. Raspet, and H. E. Bass, "Stability analysis of a helium-filled thermoacoustic engine," *J. Acoust. Soc. Am.* **96**, 370–375 (1994).
- <sup>5</sup>The heat exchangers were constructed by W. Patrick Arnott, Robert Abbott, and Michael Ossofsky at the Desert Research Institute, Reno, NV.
- <sup>6</sup>J. A. Lightfoot, "Thermoacoustic engines in alternate geometry resonators," Ph.D. Dissertation, The University of Mississippi (1997).
- <sup>7</sup>R. Raspet, J. Brewster, and H. E. Bass, "A new approximation method for thermoacoustic calculations," *J. Acoust. Soc. Am.* **103**, 2395–2402 (1998).
- <sup>8</sup>F. Reif, *Fundamentals of Statistical and Thermal Physics* (McGraw-Hill, New York, 1965), pp. 166–169.
- <sup>9</sup>J. R. Belcher, "A study of element interactions in thermoacoustic engines," Ph.D. Dissertation, The University of Mississippi (1996).
- <sup>10</sup>A. B. Coppens and J. V. Sanders, "Finite-amplitude standing waves in rigid-walled tubes," *J. Acoust. Soc. Am.* **43**, 516–529 (1968).
- <sup>11</sup>R. Chen, "Time averaged pressure distributions for finite amplitude standing waves," Master's Thesis from Pennsylvania State University, Graduate Program in Acoustics (December 1994).
- <sup>12</sup>A. A. Atchley, H. E. Bass, and T. J. Hofler, "Development of nonlinear waves in a thermoacoustic prime mover," in *Frontiers of Nonlinear Acoustics: Proceedings of 12th ISNA*, edited M. F. Hamilton and D. T. Blackstock (Elsevier, New York, 1990), pp. 603–608.
- <sup>13</sup>G. W. Swift, "Analysis and performance of a large thermoacoustic engine," *J. Acoust. Soc. Am.* **92**, 1551–1562 (1992).
- <sup>14</sup>D. F. Gaitan and A. A. Atchley, "Finite amplitude standing waves in harmonic and anharmonic tubes," *J. Acoust. Soc. Am.* **93**, 2489–2495 (1993).
- <sup>15</sup>A. B. Coppens and J. V. Sanders, "Finite-amplitude standing waves within real cavities," *J. Acoust. Soc. Am.* **58**, 1133–1140 (1975).
- <sup>16</sup>J. R. Olson and G. W. Swift, "Similitude in thermoacoustics," *J. Acoust. Soc. Am.* **95**, 1405–1412 (1994).